HHS Public Access

Author manuscript

J Neuroimaging. Author manuscript; available in PMC 2016 March 02.

Published in final edited form as:

J Neuroimaging. 2016 March ; 26(2): 240–246. doi:10.1111/jon.12281.

Comparison of Glioblastomas and Brain Metastases using Dynamic Contrast-Enhanced Perfusion MRI

Brian C. Jung, **Julio Arevalo-Perez**, **John K. Lyo**, **Andrei I. Holodny**, **Sasan Karimi**, **Robert J. Young**, and **Kyung K. Peck**

Department of Radiology, Memorial Sloan Kettering Cancer Center, New York, NY (BJ, JAP, JL, AH, SK, RY); and Department of Medical Physics, Memorial Sloan Kettering Cancer Center, New York, NY (KP).

Abstract

PURPOSE—To compare glioblastoma and brain metastases using T1-weighted dynamic contrast-enhanced (DCE)-MRI perfusion technique.

METHODS—26 patients with glioblastoma and 32 patients with metastatic brain lesions with no treatment who underwent DCE-MRI were, retrospectively, analyzed. DCE perfusion parameters K^{trans} and V_p were calculated for the whole tumor. Signal intensity time curves were quantified by calculating the area under the curve (AUC) and the logarithmic slope of the washout phase to explore the heterogeneous tumor characteristics.

RESULTS—Glioblastoma did not differ from all brain metastases in K^{trans} (P = .34) or V_p (P = .47). Glioblastoma and melanoma metastases differed from hypovascular metastases in AUC and log slope of the washout phase of the signal intensity time curve (P < .05); however, glioblastoma and melanoma metastases did not differ from each other (AUC: P = .78, Log slope: P = .77). Glioblastoma and melanoma metastases differed from hypovascular metastases in the ratio of $Voxel_{neg}/Voxel_{pos}$ (P< .03); however, they did not differ from each other. Glioblastoma and melanoma metastases differed from each other in $Voxel_{neg\_threshold}$ at higher negative log slope threshold.

CONCLUSION—DCE-MRI showed that it has a potential to differentiate glioblastomas, melanoma metastases and hypovascular brain tumors. Logarithmic slope of the washout phase and AUC of the signal intensity time curve were shown to be the best discriminator between hypervascular and hypovascular neoplasms.

Keywords

Glioblastoma; dynamic contrast-enhanced (DCE) MRI; metastasis; brain; neoplasm

Correspondence: Address correspondence to Kyung K. Peck, Department of Radiology, Memorial Sloan Kettering Cancer Center, 1275 York Avenue, New York, NY 10065, United States. peckk@mskcc.org.

Introduction

Glioblastoma and metastatic brain tumors are the two most common malignant brain tumors. Clinical management and prognosis vary vastly between the two pathologies. However, it is often difficult to differentiate between these two entities on the conventional MR imaging.[1] Metastatic brain lesions can often be strongly suspected based on the presence of a malignant primary or multiplicity of lesions. However, many instances of brain metastases initially present as a single, isolated lesion. Glioblastomas can present as multiple lesions. Furthermore, previous studies suggest that patients with a primary cancer of nonbrain origin could genetically be at a higher risk of developing primary glioblastoma as compared to the general population risk thereby complicating the proper diagnosis.[2–7] In addition, it is always preferable to establish an accurate diagnosis without having to resort to a brain biopsy, especially if the lesion is in an especially dangerous part of the brain or if treatment does not require resection. Therefore, a quantitative imaging biomarker that could differentiate primary glioblastoma from secondary metastatic tumor could provide substantial improvement in the clinical management of brain tumors.

Dynamic contrast-enhanced (DCE) MRI is an emerging advanced imaging technique that provides physiological information such as tumor vascularity and hemodynamic characteristics of the neoplasm that is unavailable with the conventional MR imaging. DCE-MRI has been demonstrated to be a potentially useful biomarker that can differentiate low versus high-grade gliomas,[8] evaluate the effects of antiangiogenic therapy[9,10] and radiation therapy,[11] and differentiate recurrent glioblastoma from radiation necrosis.[12] Semiquantitative analysis of the signal intensity time curve using DCE-MRI has also been shown to be an important clinical biomarker in differentiating benign from malignant lesions in the prostate[13] and orbital masses.[14] In breast neoplasms, Kuhl et al demonstrated that rapid washout of the contrast agent in DCE-MRI was characteristic of malignant lesions while benign neoplasms showed a slower washout of the contrast agent.[15] The morphological analysis of the signal intensity time curve has also been applied to studying the neoplasms of the brain. Bagher-Ebadian et al proposed that there exists four different patterns of signal intensity time curve and that the different regions of the brain in glioblastoma patients showed a different pattern of signal intensity time curve.[16] However, to our knowledge, there has not been a study that investigates the use of DCE-MRI pharmacokinetic parameters and semiquantitative analysis of the signal intensity time curve to characterize the perfusion differences between glioblastoma, hypervascular brain metastases, and hypovascular brain metastases.

In this study, our goal was to evaluate glioblastoma, melanoma, and other brain metastases using T1-weighted DCE-MRI perfusion technique. Since glioblastoma and melanoma metastases are both hypervascular tumors, we hypothesized that glioblastoma and melanoma metastases would differ from other hypovascular metastases on perfusion parameters, while glioblastoma and melanoma would not differ from each other.

Methods

Patient Demographics

This retrospective study was authorized by the institutional review board. This was in full compliance with all Health Insurance Portability and Accountability Act regulations. As this was a retrospective review, informed consent was waived. Consecutive patients with known primary glioblastoma, and brain metastases who had completed a DCE-MRI examination between 2011 and 2014 were identified from an institutional database. Diagnosis was established by histopathology of the brain lesion. Patients who received surgical resection, radiation therapy, corticosteroids, or antiangiogenic therapy prior to their DCE-MRI scan were excluded. The final cohort of 58 patients consisted of patients with primary glioblastoma (n = 26), hypervascular brain metastases (of melanoma origin n = 16), and hypovascular brain metastases (n = 16, including nonsmall cell lung [n = 7], breast [n = 6], and colon [n = 3]).

MRI Acquisition

MRI sequences were acquired with a 1.5-T or 3.0-T scanner (GE Healthcare, Milwaukee, WI) and a standard eight-channel head coil. T1-weighted DCE-MRI of the brain was acquired as a part of standard clinical protocol. A bolus of gadobutrol (Gadavist, Bayer Healthcare, Leverkusen, Germany) at .1-mmol/kg was administered by a power injector at a rate of 2–3 mL/second.

The kinetic enhancement of tissue during and after injection of Gd-DTPA was obtained using a 3-D T1-weighted fast spoiled-gradient (SPGR) echo sequence: TR 4–5 ms; TE 1–2 ms; slice thickness 3 mm; FA 25°; FOV 24 cm; matrix 256 × 128; temporal resolution (Δt) of 5–6 s. Ten to fourteen slices covering the lesion were scanned over 40 phases, with the injection occurring after the first ten phases. Matching T1-weighted (TR 600 ms; TE 8 ms; slice thickness 4.5 mm) and T2-weighted (TR 4000 ms; TE 102 ms; slice thickness 4.5 mm) spin-echo images were obtained.

Image Analysis

Data processing and the analysis of pharmacokinetic variables were conducted using NordicICE version 2 (NordicNeuroLab, Bergen, Norway). This applies a pharmacokinetic model of contrast uptake to the calculated signal intensity changes over time. Using a two-compartment kinetic model, the contrast agent is presumed to be distributed in the blood plasma volume, leaking in a time-dependent manner into the interstitium.[17] Time-dependent leakage (K^{trans}) and the blood plasma volume (V_p) were calculated using Toft's pharmacokinetic model analysis[17] on a voxel-by-voxel basis. Preprocessing included removal of background noise and deconvolution with the arterial input function (AIF). Linear assumption was made between change in signal intensity and gadolinium concentration to convert signal intensity curve to concentration-time curve. The AIF was obtained from middle cerebral artery independently for every patient. Curves showing an optimal relationship between AIF and concentration-time curve were carefully selected.

All regions-of-interest (ROIs) were manually delineated by a trained operator, who was blind to patient data and tumor histology, on the axial T1 postcontrast scans. The borders of the lesions were defined as the edge of the contrast enhancement on the T1 postcontrast scan. ROI included the enhancing tumor tissue as well as the regions of cystic and/or necrotic change, but excluded adjacent vessels. Since tumors spanned across multiple axial slices, an ROI was drawn on each axial slice and the values were calculated for each slice, and then, averaged to create a volume of interest (VOI) for the whole tumor.

Permeability, Plasma Volume, and Tumor Response Signal Intensity Time Curve—Time-dependent leakage (K^{trans}) and the blood plasma volume (V_p) were calculated using Tofts pharmacokinetic model analysis[17] on a voxel-by-voxel basis using the NordicICE software. VOIs from the postcontrast scans were then transferred to the parametric maps (K^{trans} and V_p) to calculate the mean of each perfusion parameter for the whole tumor.

To conduct a semiquantitative analysis, the tumor response signal intensity curve was analyzed. Signal intensity (SI) time curve measures the concentration of the contrast agent detected in each voxel with respect to time. To minimize the effect of noise, we calculated the mean SI time curve using a moving-average technique using proprietary software based in MATLAB (R2014a, Natick, MA). We used VOIs composed of 2×2×2 voxels and calculated the mean SI time curve only from VOIs that had at least 50% of the voxels (>4 voxels) included inside the manually delineated VOI in order to minimize noise.

The VOI of maximal enhancement was then identified. The enhancement value was defined as the percent change in SI between the preinjection time point and the maximum signal intensity. Since some of the voxels showed a gradual increase in SI throughout the entire duration of the scan rather than a clear decay in signal in the washout phase, we determined the maximum SI value to be the maximum signal value between 90 and 130 seconds after the injection of contrast. This was based on the fact that all SI time curves included the maximum values within that range of time. All the SI time curves were then expressed as a function of % SI, with SI value at the time point of maximum enhancement as 100%. The washout phase of the SI time curve was determined as the time between the time point of maximal SI and the end of the scan acquisition.

To compare the morphology of the SI time curves between the different tumor types, we calculated the area under the curve (AUC) of the SI time curve and the logarithmic slope of the washout phase at the region of maximal enhancement. AUC of the SI time curve was computed using the trapezoidal numerical integration method (*trapz.m*, MATLAB R2014a). The washout phase was characterized using the logarithmic scale in order to account for the exponentially decaying nature of the washout phase (fast initial decay followed by a slower rate of decay in signal intensity). We used a first-order polynomial fit to determine the logarithmic slope. In regions that had poor linear fitting ($P > .05$), the logarithmic slope of washout phase of the region was assigned as 0.

We further semiquantitatively classified the morphology of the SI time curve into three subtypes. Type I was classified as the SI time curves that showed an increasing washout

phase (log slope of the washout phase > 1). Type III was classified as the SI time curves that demonstrated a decreasing washout phase (log slope of the washout phase < −1). The SI time curves that showed poor linear fitting ($P > .05$) in the washout phase or had log slope of the washout phase between −1 and 1 were classified as Type II (plateau washout phase).

Spatial Heterogeneity within the Different Tumor Types—To study the spatial heterogeneity within the different tumor types, we calculated the SI time curve for each voxel within the tumor. Only scans that covered the entire tumor in the cranio-caudad direction were analyzed. Each voxel within the tumor was then classified as either $Voxel_{neg}$ or $Voxel_{pos}$ based on the value of the logarithmic slope of the washout phase (log slope <0: $Voxel_{neg}$; log slope >0: $Voxel_{pos}$). As part of a post hoc analysis, we calculated the number of $Voxel_{neg}$ at different negative washout log slope thresholds. The different slope thresholds were chosen by first calculating the maximum absolute negative washout log slope from the entire sample pool, and then, setting the threshold at 40 equivalent increments from 0 to maximum absolute negative washout log slope. For each incremental slope threshold, we calculated $Voxel_{neg\_threshold}$, which was defined as the number of $Voxel_{neg}$ that had the washout log slope < threshold (the washout phase is decaying at a higher rate than the threshold). The same method was applied to calculate $Voxel_{pos\_threshold}$ for the number of $Voxel_{pos}$ at different positive washout log slope thresholds. The ratio of $Voxel_{neg\_threshold}/Voxel_{neg}$ and $Voxel_{pos\_threshold}/Voxel_{pos}$ was plotted against the incremental changes in the slope threshold, and the AUC was calculated as an index to compare the heterogeneity between the different tumor pathologies. Mann-Whitney U test was used to compare the difference in $Voxel_{neg\_threshold}$ and $Voxel_{pos\_threshold}$ between the different disease groups.

Statistical Analysis

Intergroup differences in the pharmacokinetic variables (K^{trans} and V_p) and the SI time curve characteristics (AUC and logarithmic slope of the washout phase) were compared using the Mann-Whitney U test. Receiver operating characteristic (ROC) curve analysis was used to assess the discriminatory power of each variable in differentiating between the different tumor pathologies.

Results

Permeability, Plasma Volume, and Tumor Response Signal Intensity Time Curve

As compared to the hypovascular metastases, the hypervascular tumors (glioblastoma and melanoma metastases) showed an increase in AUC of the SI time curve (Fig 1A) and the log slope of the washout phase (Fig 1B). Glioblastoma did not differ from melanoma metastases (melanoma) (AUC: $P = .814$; log slope: $P = .972$). Pharmacokinetic variables did not differ between the three tumor pathologies (Table 1).

ROC analysis of the pharmacokinetic variables and the SI time curve characteristics (Fig 2) showed that AUC of the SI time curve and the log slope of the washout phase could successfully differentiate hypovascular metastases from both types of hypervascular neoplasms (glioblastomas and melanoma metastases). AUC and the log slope of the washout

phase could not differentiate between glioblastoma and metastatic melanoma. Neither of the pharmacokinetic variables could discriminate between the three tumor pathologies. The optimal cutoff and AUC of the ROC analysis are listed in Table 2.

Consistent with the results of the Mann-Whitney U test, our semiquantitative analysis showed that at the region of maximal enhancement, hypovascular tumors demonstrated an increased number of Type III pattern (45.5% in hypovascular metastases, 8.7% in glioblastoma, and 7.1% in melanoma metastases). In contrast, glioblastoma and melanoma metastases showed an increased number of Type II pattern (glioblastoma: 60.9%, melanoma metastases: 64.3%, hypovascular metastases: 36.4%) or Type I pattern (glioblastoma: 30.4%, melanoma metastases: 28.6%, hypovascular metastases: 18.2%) of the washout phase (Fig 3).

Spatial Heterogeneity within the Different Tumor Types

The scans that covered the entire height of the tumor included 23 glioblastomas, 14 melanoma metastases, and 11 hypovascular metastases. A comparison of the ratio ($Voxel_{neg}/Voxel_{pos}$) showed that hypovascular metastases ($\bar{x}_{hypovascular} = 13.9$) had an increased proportion of voxels that were $Voxel_{neg}$ as compared to glioblastoma ($\bar{x}_{glioblastoma} = 6.8$, $P = .03$). Hypovascular metastases also showed an increased number of $Voxel_{neg}$ as compared to melanoma metastases ($\bar{x}_{melanoma} = 4.2$), however, this difference was not statistically significant ($P = .11$). Glioblastoma did not differ from melanoma metastases ($P = .34$).

We then repeated the analysis at different slope thresholds. We classified each voxel as $Voxel_{neg\_threshold}$ if the log slope of the washout phase of the voxel was lower than the threshold value. A plot of the number of $Voxel_{neg\_threshold}$ versus the change in the negative log slope threshold is shown in Figure 4. As expected, the number of $Voxel_{neg\_threshold}$ and $Voxel_{pos\_threshold}$ were lower at higher cutoff thresholds. The Mann-Whitney U test showed that at higher negative log slope thresholds (more negative log slope cutoff), glioblastoma trended towards having a greater number of $Voxel_{neg\_threshold}$ as compared to melanoma ($P = .07$). Glioblastoma and melanoma metastases did not differ from the hypovascular metastases ($P = .17$). When $Voxel_{neg\_threshold}/Voxel_{neg}$ was plotted with respect to the different slope thresholds (Fig 4), we found that glioblastoma and melanoma metastases trended towards differing in the AUC of this curve ($P = .07$). Neither glioblastoma nor melanoma metastases differed from hypovascular metastases ($P = .17$ and $P = .89$, respectively).

Discussion

In this study, we evaluated the use of DCE-MRI in the differentiation of glioblastoma, melanoma brain metastases, and other hypovascular brain metastases. Our findings show that while pharmacokinetic variables cannot discriminate between the three tumor pathologies, quantitative assessment of the signal intensity time curve could differentiate hypovascular metastases from glioblastomas and melanoma metastases. Out of the four parameters we investigated, the log slope of the SI washout phase was shown to be the best discriminator between the three tumor pathologies. Our findings also showed that that there

may exist heterogeneity in the spatial pattern of the SI washout phase throughout the entire tumor.

Glioblastoma and Melanoma Metastases Differ from Hypovascular Tumors, but not from Each Other

Our findings demonstrate that at the region of maximal enhancement, glioblastoma and melanoma metastases both differed from hypovascular metastases in the pattern of SI time curve; however, glioblastoma and melanoma metastases did not differ from each other. This is consistent with previous findings in the spinal metastases, which show that DCE-MRI can differentiate between hypervascular and hypovascular tumors.[18] The lack of difference between glioblastoma and melanoma metastases in DCE-MRI may indicate that despite the different process of angiogenesis thatmay occur, DCE-MRI lacks sensitivity to discriminate between the different types of hypervascular neoplasms.

More specifically, we found that the best discriminating factor in differentiating between hypervascular and hypovascular tumors are the morphological characteristics of the signal intensity time curves (AUC and log slope of the washout phase) at the region of maximal enhancement. It is yet unclear why different morphological types of signal intensity time curves exist. It has been hypothesized that the regions of the tumor that show a decaying pattern of washout is associated with an increased leakiness of the contrast agent, presumably caused by increased microvessel density and arteriovenous anastomoses.

While our results show that the morphology of the signal intensity time curve could serve as a biomarker to differentiate between tumor types, further study is necessary to investigate its prognostic power across different pathologies. Previous studies in breast cancer have demonstrated that tumors that are characterized by a decaying pattern of washout are more likely to be malignant as compared to tumors with an increasing pattern of washout phase.[15] However, comparing the prognosis across the different tumor types based on the morphology of the signal intensity time curve alone is beyond the scope of this study.

Unlike the previous study on breast cancer that studied a single homogenous pathology, our study sample included a heterogeneous group of mixed tumor types. It is possible that hypervascular and hypovascular tumors all lie in one spectrum and could be compared against each other based on the shape of the signal intensity time curve. On the contrary, it is also possible that there exists a separate spectrum for each different type of tumor and the comparison between different tumor types is not possible. Therefore, while we found more decaying pattern of washout phase in the hypovascular tumors, this may not necessarily be an indication of increased tumor malignancy in the hypovascular tumors as compared to the hypervascular neoplasms.

The Morphology of the Signal Intensity Time Curve is Spatially Heterogeneous

Qualitatively, we found that most tumors had both the regions of decaying washout and the regions of increasing washout pattern throughout the entire tumor volume. Interestingly, upon visual inspection, we observed that regions of increasing washout pattern were more concentrated towards the core of the tumor, whereas the regions of decaying washout pattern clustered towards the rim of the tumor. If decaying pattern of washout phase is indeed an

indicator of tumor malignancy and aggressiveness, it is possible that the regions of decaying washout pattern in the periphery of the tumor is responsible for the increase in tumor mass with the progression of disease. Longitudinal investigation of the morphology of the signal intensity time curve after surgical resection or radiation therapy could provide us with an insight into developing a probabilistic model of the tumor recurrence.

This spatial pattern of the signal intensity time curve is in contrast to the findings of Bagher-Edbadian et al in glioblastoma patients, which showed an increasing washout pattern towards the rim of the tumor while central regions of necrosis showed a decaying washout pattern in the signal intensity time curve.[16] This discrepancy could have occurred because while our analyses focused on the washout phase of the signal intensity time curve only, Bagher-Edbadian et al classified the regions based on the morphologic characteristics of both the wash-in and the washout phase of the signal intensity time curve. Furthermore, Bagher-Edbadian et al did not normalize the signal intensity time curve in their analyses. Therefore, the regions classified as increasing washout pattern by Bagher-Edbadian could have been a result of a combination of high peak enhancement as well as the increasing pattern of the washout phase. In contrast, our findings focused only on the morphology of the washout phase of the signal intensity time curve after normalizing the signal intensity time curve, which could have yielded contrasting results.

Our findings showed that at higher negative log slope thresholds for the washout phase of the signal intensity time curves, glioblastoma had a greater number of regions with decaying pattern of washout phase than melanoma metastases. This suggests that rather than classifying the brain region as either increasing or decreasing washout phase, future studies should focus on performing heterogeneity pattern analysis of the tumor to compare both the morphology of the signal intensity time curve as well as its spatial heterogeneity in order to differentiate between different pathologies.

Limitations of the Study

This study had several potential limitations. First, the study was conducted, retrospectively, and the post hoc moving average analyses were only performed on a subset of the patients. Nevertheless, we observed significant results that have prompted future prospective study. Second, the tumor volumes were manually delineated. Despite this, any potential variation in reproducibility was mitigated by having a single trained operator perform all VOIs. Third, although there are other hypervascular metastases such as thyroid, renal cell carcinoma (RCC), the hypervascular metastases group was limited to melanoma. This circumstance could not be avoided, because brain metastasis of melanoma origin are more common among the general population, and we recruited consecutive patients. Fourth, T1 mapping was not performed to estimate T1 values for each pixel during preinjection period. Instead, a fixed T1 (1000 ms) value was used assuming blood and tissue have a linear relationship. However, T1 mapping would be a proper approach if nonlinear relationship is considered, due to the heterogeneity of the enhancing lesions. Finally, in our study 1.5-T and 3-T scanners were used to acquire DCE data. Modeled variables in Tofts model are in theory independent of the scanning acquisition protocol including field strength, thus avoiding problems associated with signal intensity metrics.[19,20]

Conclusion

DCE-MRI can be used to differentiate hypervascular neoplasms from hypovascular metastatic brain tumors. Logarithmic slope of the washout phase and the AUC of the signal intensity time curve were shown to be the best discriminator between hypervascular and hypovascular neoplasms. Our results showed that the pattern of the washout phase of the signal intensity time curve is spatially heterogeneous. This could aid in the differentiation of tumor types as well as in the clinical management of brain tumors.

References

1. Campos S, Davey P, Hird A, et al. Brain metastasis from an unknown primary, or primary brain tumour? A diagnostic dilemma. Curr Oncol. 2009; 16:62–66. [PubMed: 19229374]
2. Pratt CB, Meyer WH, Luo X, et al. Second malignant neoplasms occuring in survivors of osteosarcoma. Cancer. 1997; 80:960–965. [PubMed: 9307198]
3. Liaw D, Marsh DJ, Li J, et al. Germline mutations of the PTEN gene in Cowden disease, an inherited breast and thyroid cancer syndrome. Nature Genetics. 1997; 16:64–67. [PubMed: 9140396]
4. Li J, Yen C, Liaw D, et al. PTEN, a putative protein tyrosine phosphatase gene mutated in human brain, breast, and prostate cancer. Science. 1997; 275:1943–1947. [PubMed: 9072974]
5. Elmariah SB, Huse J, Mason B, et al. Multicentric glioblastoma multiforme in a patient with BRCA-1 invasive breast cancer. Breast J. 2006; 12:470–474. [PubMed: 16958968]
6. Lorenzo Bermejo J, Hemminki K. Risk of cancer at sites other than the breast in Swedish families eligible for BRCA1 or BRCA2 mutation testing. Ann Oncol. 2004; 15:1834–1841. [PubMed: 15550590]
7. Piccirilli M, Salvati M, Bistazzoni S, et al. Glioblastoma multiforme and breast cancer: report on 11 cases and clinico-pathological remarks. Tumori. 2005; 91:256–260. [PubMed: 16206651]
8. Jung SC, Yeom JA, Kim JH, et al. Glioma: Application of histogram analysis of pharmacokinetic parameters from T1-weighted dynamic contrast-enhanced MR imaging to tumor grading. AJNR Am J Neuroradiol. 2014; 35:1103–1110. [PubMed: 24384119]
9. Jalali S, Chung C, Foltz W, et al. MRI biomarkers identify the differential response of glioblastoma multiforme to anti-angiogenic therapy. Neuro Oncol. 2014; 16:868–879. [PubMed: 24759636]
10. Gossmann A, Helbich TH, Kuriyama N, et al. Dynamic contrast-enhanced magnetic resonance imaging as a surrogate marker of tumor response to anti-angiogenic therapy in a xenograft model of glioblastoma multiforme. J Magn Reson Imaging. 2002; 15:233–240. [PubMed: 11891967]
11. Hawighorst H, Knopp MV, Debus J, et al. Pharmacokinetic MRI for assessment of malignant glioma response to stereotactic radiotherapy: initial results. J Magn Reson Imaging. 1998; 8:783–788. [PubMed: 9702878]
12. Chung WJ, Kim HS, Kim N, et al. Recurrent glioblastoma: optimum area under the curve method derived from dynamic contrast-enhanced T1-weighted perfusion MR imaging. Radiology. 2013; 269:561–568. [PubMed: 23878286]
13. Ren J, Huan Y, Wang H, et al. Dynamic contrast-enhanced MRI of benign prostatic hyperplasia and prostatic carcinoma: correlation with angiogenesis. Clin Radiol. 2008; 63:153–159. [PubMed: 18194690]
14. Yuan Y, Kuai XP, Chen XS, et al. Assessment of dynamic contrast-enhanced magnetic resonance imaging in the differentiation of malignant from benign orbital masses. Eur J Radiol. 2013; 82:1506–1511. [PubMed: 23561057]
15. Kuhl CK, Mielcareck P, Klaschik S, et al. Dynamic breast MR imaging: are signal intensity time course data useful for differential diagnosis of enhancing lesions? Radiology. 1999; 211:101–110. [PubMed: 10189459]
16. Bagher-Ebadian H, Jain R, Nejad-Davarani SP, et al. Model selection for DCE-T1 studies in glioblastoma. Magn Reson Med. 2012; 68:241–251. [PubMed: 22127934]

17. Tofts PS, Brix G, Buckley DL, et al. Estimating kinetic parameters from dynamic contrast-enhanced T(1)-weighted MRI of a diffusable tracer: standardized quantities and symbols. J Magn Reson Imaging. 1999; 10:223–232. [PubMed: 10508281]
18. Khadem NR, Karimi S, Peck KK, et al. Characterizing hypervascular and hypovascular metastases and normal bone marrow of the spine using dynamic contrast-enhanced MR imaging. AJNR Am J Neuroradiol. 2012; 33:2178–2185. [PubMed: 22555585]
19. Jackson A, O'Connor JP, Parker GJ, et al. Imaging tumor vascular heterogeneity and angiogenesis using dynamic contrast-enhanced magnetic resonance imaging. Clin Cancer Res. 2007; 13:3449–3459. [PubMed: 17575207]
20. Tofts PS. T1-weighted DCE imaging concepts: modelling, acquisition and analysis. MAGNETOM Flash 3/2010. :30–39.

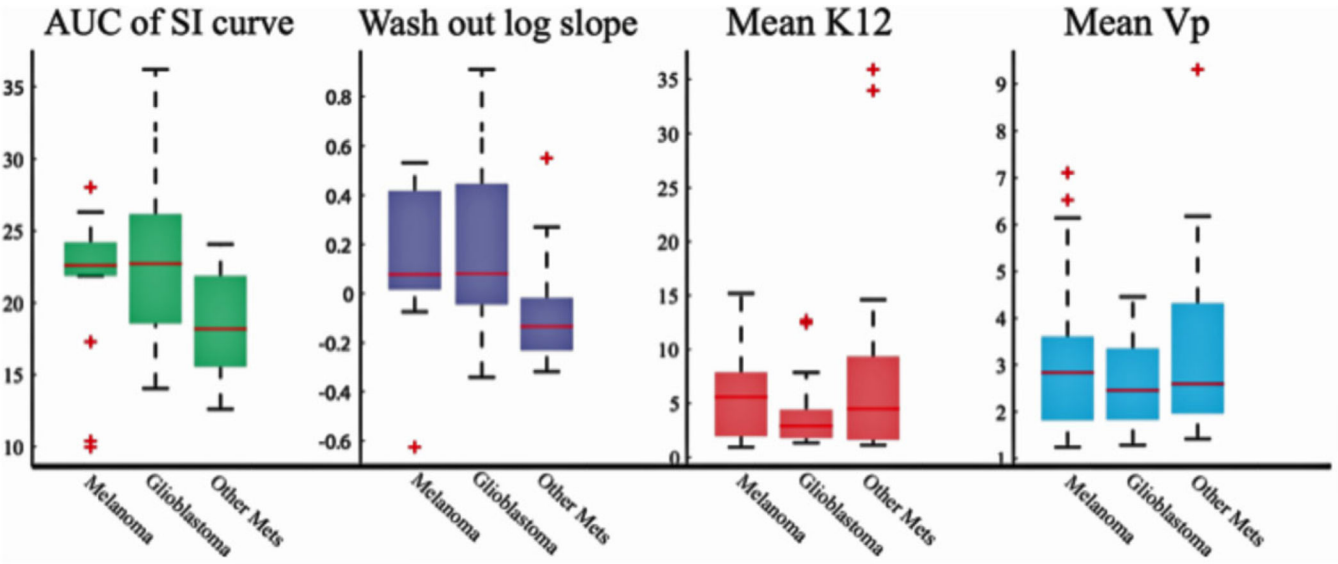

Fig 1.

The morphology of the signal intensity time curve could differentiate hypervascular brain tumors from hypovascular brain tumors: Hypervascular brain tumors (glioblastoma and melanoma metastases) differed from hypovascular brain metastases in the AUC and the logarithmic slope of the washout phase of the signal intensity time curve; however, glioblastoma and melanoma metastases could not be differentiated from each other based on the morphological characteristics of the signal intensity time curve. K^{trans} and V_p could not differentiate between the three pathologies.

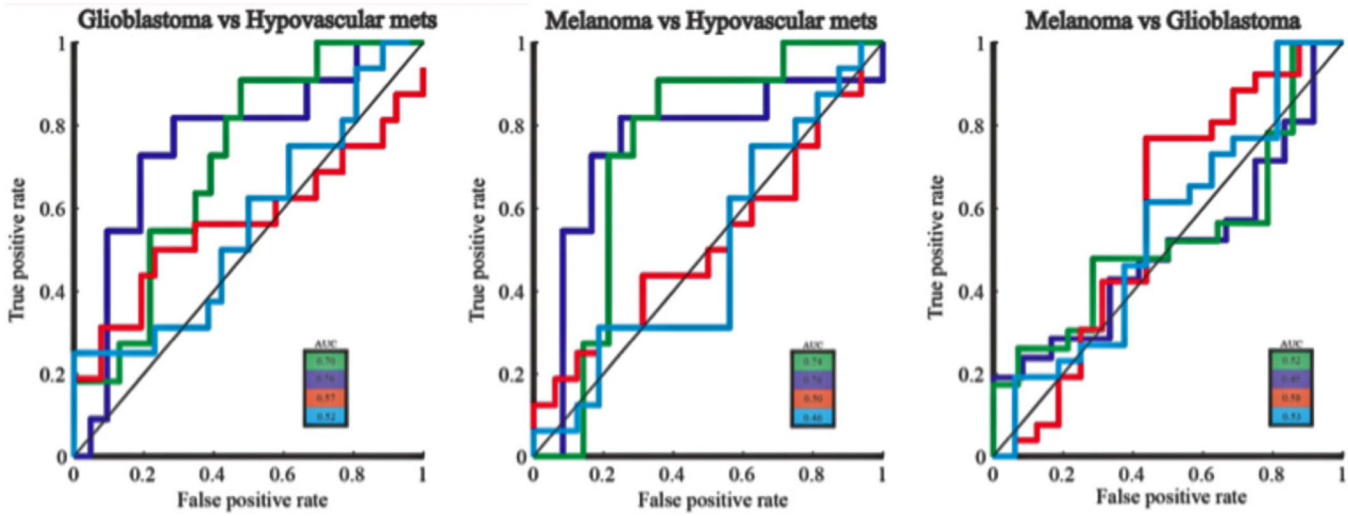

Fig 2.

ROC curve shows that AUC and log slope of the washout phase could successfully discriminate between hypervascular neoplasms from hypovascular metastases: ROC analysis showed that the logarithmic slope of the washout phase had the highest discriminatory power in differentiating hypervascular tumors (glioblastoma and melanoma) from hypovascular metastases (AUC = .76), followed by the AUC of the signal intensity time curve (AUC = .70 and .74, respectively). Neither of these two variables could differentiate glioblastoma from metastatic melanoma (AUC ≤ .52).

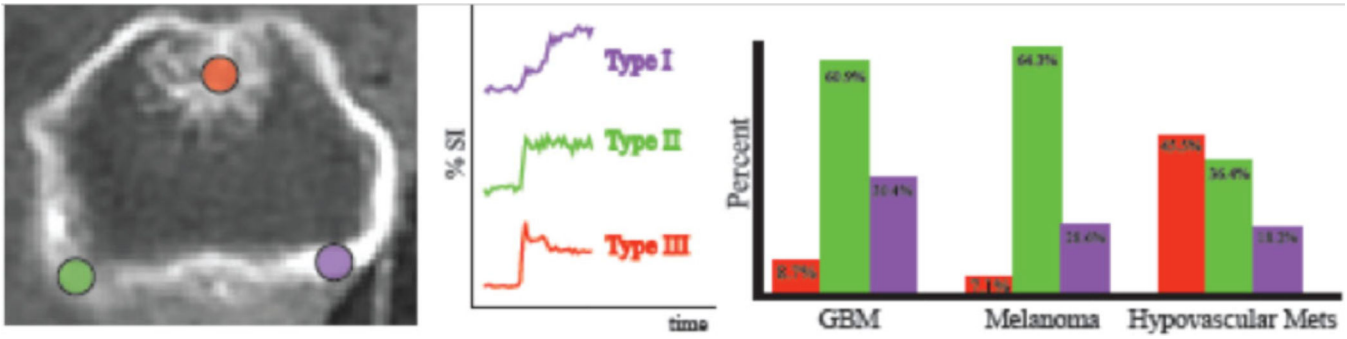

Fig 3.

Perfusion characteristics at the region of maximal enhancement: At the region of maximal enhancement, hypovascular metastases showed an increased number of type III signal intensity time curves, while both types of hypervascular tumors showed greater number of type I and II morphology.

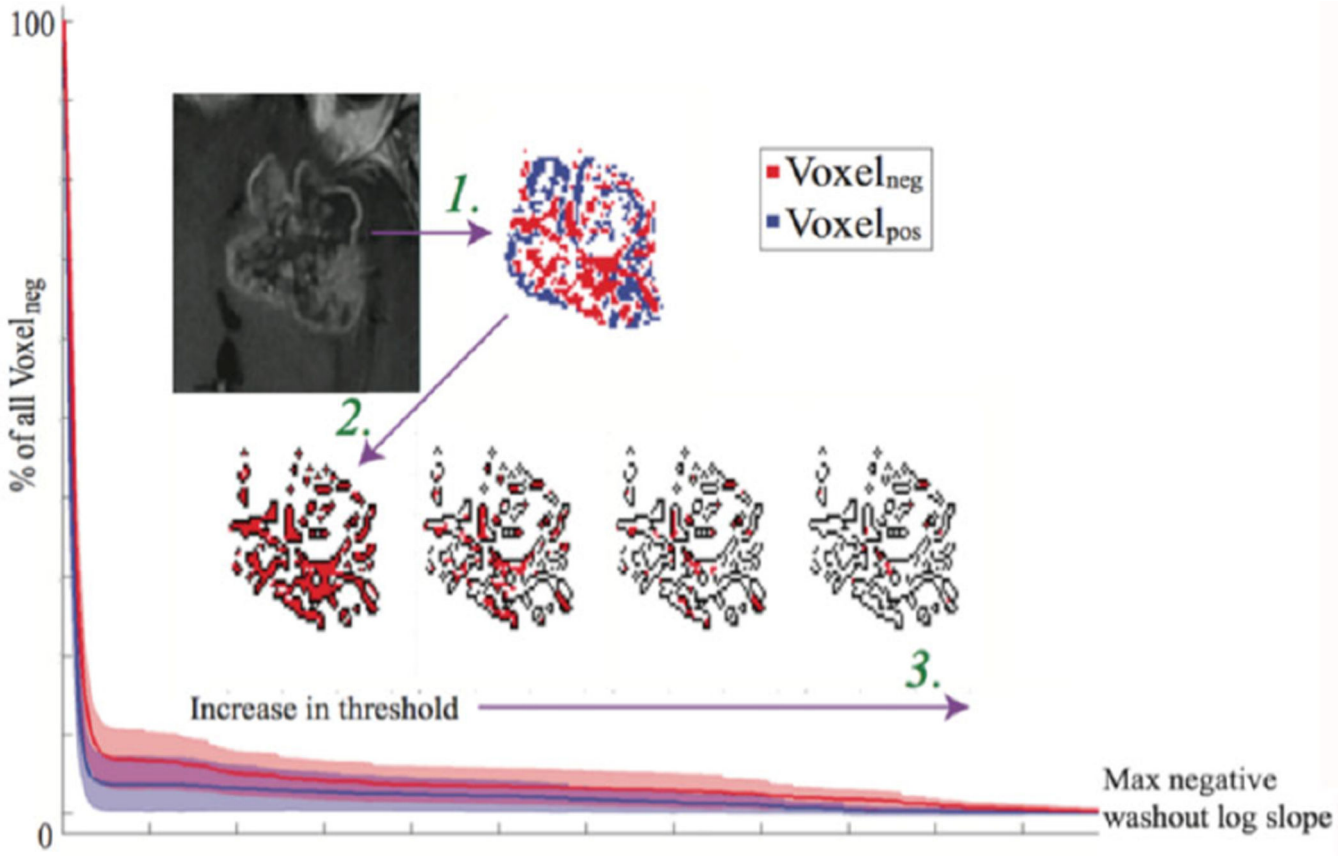

Fig 4.

Glioblastoma shows increased number of $Voxel_{neg}$ at higher negative log slope threshold: Logarithmic slope of the washout phase of the signal intensity time curve was calculated for each voxel within the tumor region. Arrow #1: Each voxel was then classified as $Voxel_{neg}$ or $Voxel_{pos}$ based on the value of the logarithmic slope ($Voxel_{neg}$ = [log slope < 0]; $Voxel_{pox}$ = [log slope > 0]). Voxels that showed poor linear correlation in the washout phase were excluded from the analysis. Arrow #2: All the $Voxel_{neg}$ were then selected for further analysis (total number of $Voxel_{neg}$; *threshold* = 0). Arrow #3: The $Voxel_{neg}$ was then calculated at different negative slope thresholds ($Voxel_{neg\_threshold}$ = [log slope < *threshold*], $Voxel_{plateau\_threshold}$ = [*threshold* < log slope < 0], $Voxel_{pox\_threshold}$ = [log slope > *threshold*]). The number of $Voxel_{neg\_threshold}$ at different threshold (red filled pixels) was then expressed as a fraction of the total number of $Voxel_{neg}$ (black outline). At higher threshold values, glioblastoma showed an increased ratio of ($Voxel_{neg\_threshold}$/$Voxel_{neg}$) than melanoma metastases. The ratio ($Voxel_{neg\_threshold}$/$Voxel_{neg}$) was plotted against the negative washout log slope threshold. As compared to melanoma metastases, the AUC trended towards being increased in glioblastoma patients (P = .072). There was no difference in the AUC between glioblastoma and hypovascular metastases (P = .173) or between melanoma metastases and hypovascular metastases (P = .891).

Table 1

AUC and the Washout Log Slope can Differentiate Glioblastoma and Melanoma Metastases from Hypovascular Metastases, but not from Each Other

	AUC	Washout Log Slope	K_{trans}	V_p
GBM versus Melanoma	.790	.772	.386	.614
GBM versus Hypovascular Mets	.047*	.019*	.493	.493
Melanoma versus Hypovascular Mets	.046*	.024*	.865	.955

Hypervascular tumors showed increased AUC and washout log slope in the signal intensity time curve as compared to hypovascular tumors. Pharmacokinetic variables (K_{trans} and V_p) did not differ between the two pathologies. Glioblastoma and melanoma did not differ from each other in all four parameters.

* Significant results ($P < .05$).

Table 2

The Optimal Cutoff Value for ROC Analysis

	AUC	Washout Log Slope
GBM versus Hypovascular Mets	22.15	−0.04
Melanoma versus Hypovascular Mets	22.11	0.01

ROC analysis of the AUC showed that for GBM versus hypovascular metastases, sensitivity and specificity were optimized by a cutoff point at 22.15, while the cutoff point was 22.11 for melanoma metastases versus hypovascular metastases. The optimal cutoff point for the washout log slope was –0.04 for GBM versus hypovascular metastases and 0.01 for melanoma metastases versus hypovascular metastases.